Author Manuscript

Author Manuscript

Author Manuscript

Author Manuscript

HHS Public Access

Author manuscript

*Lab Chip*. Author manuscript; available in PMC 2019 July 10.

Published in final edited form as:

*Lab Chip*. 2018 July 10; 18(14): 2077–2086. doi:10.1039/c8lc00320c.

# Pneumatic microfluidic cell compression device for high-throughput study of chondrocyte mechanobiology

**Donghee Lee**[a,‡], **Alek Erickson**[b], **TaeSun You**[c], **Andrew T. Dudley**[b,*], and **Sangjin Ryu**[a,d,*]

[a]Department of Mechanical and Materials Engineering, University of Nebraska-Lincoln, Lincoln, NE 68588

[b]Department of Genetics, Cell Biology and Anatomy, University of Nebraska Medical Center, Omaha, NE 68198

[c]Houston District, Texas Department of Transportation, Houston, TX 77007

[d]Nebraska Center for Materials and Nanoscience, University of Nebraska-Lincoln, Lincoln, NE 68588

[‡]Current affiliation: Department of Genetics, Cell Biology and Anatomy, University of Nebraska Medical Center, Omaha, NE 68198

## Abstract

Hyaline cartilage is a specialized type of connective tissue that lines many moveable joints (articular cartilage) and contributes to bone growth (growth plate cartilage). Hyaline cartilage is composed of a single cell type, the chondrocyte, which produces a unique hydrated matrix to resist compressive stress. Although compressive stress has profound effects on transcriptional networks and matrix biosynthesis in chondrocytes, mechanistic relationships between strain, signal transduction, cell metabolism, and matrix production remain superficial. Here, we describe development and validation of a polydimethylsiloxane (PDMS)-based pneumatic microfluidic cell compression device which generates multiple compression conditions in a single platform. The device contained an array of PDMS balloons of different sizes which were actuated by pressurized air, and the balloons compressed chondrocytes cells in alginate hydrogel constructs. Our characterization and testing of the device showed that the developed platform could compress chondrocytes with various magnitudes simultaneously with negligible effect on cell viability. Also, the device is compatible with live cell imaging to probe early effects of compressive stress, and it can be rapidly dismantled to facilitate molecular studies of compressive stress on transcriptional networks. Therefore, the proposed device will enhance the productivity of chondrocyte mechanobiology studies, and it can be applied to study mechanobiology of other cell types.

## Table of contents entry:

[*]Corresponding authors.

Conflicts of interest

There are no conflicts of interest to declare.

[†]Electronic Supplementary Information (ESI) available: See DOI: 10.1039/x0xx00000x

Author Manuscript Author Manuscript Author Manuscript Author Manuscript

We demonstrate a pneumatically operated microfluidic device that can apply compressive stress of various magnitudes to multiple alginate-chondrocyte constructs simultaneously.

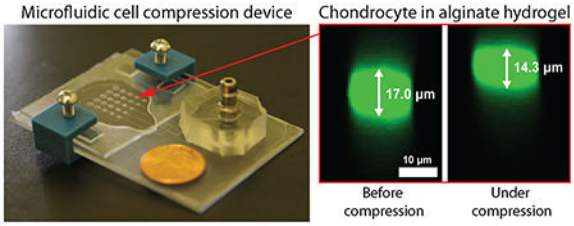


## Introduction

Many cells in the human body continuously experience various mechanical stimuli. For example, blood flow induces shear stress on vessel walls, and muscles are often in a state of contraction or stretch. There is a growing body of evidence that these mechanical stimuli are crucial for tissue homeostasis and may be essential elements that guide tissue morphogenesis during embryonic and early post natal life.[1] Also, changes in cell or matrix mechanics can lead to tissue dysfunction and disease. For example, reduced loading results in bone loss in astronauts[2] and may contribute to bone growth defects.[3–5] The impact of mechanical stimuli on cells is dependent on many factors, including scalar and vector components of force, composition and properties of the extracellular matrix (ECM) through which stress is propagated, and specific properties of the cytoskeleton and signaling networks in the target cell.[1, 6, 7]

Compressive stress is one of the major factors acting on hyaline cartilage (articular and growth plate cartilage) in which chondrocytes are the only existing cell type. To reveal the detailed mechanobiological behavior of chondrocytes under compression, macroscopic compression equipment has been used to compress chondrocytes in hydrogel or cartilage explants.[8–14] Because those macroscopic compression devices can compress a sample with a specific pair of magnitude and frequency at a time, they have limitations in testing various experimental conditions simultaneously.

To enable high-throughput mechanobiology studies of chondrocytes under multiple compressive stress conditions, we have developed a pneumatically operated microfluidic cell compression device. Microfluidic devices[15–17] are one of the popular engineered tools for studying cellular mechanobiology because they provide efficient ways to simulate *in vivo* cellular environment and to analyse cellular behaviors under various mechanical stimuli, such as shear stress,[16, 18, 19] stretch,[20, 21] compression,[22] and stiffness.[23] Also, microfluidic devices can easily integrate with optical imaging systems because of their transparent materials including polydimethylsiloxane (PDMS) and glass. With these mentioned advantages, microfluidic devices enable examining cellular behaviors under a controlled environment.

For our microfluidic cell compression device (Fig. 1a-c), we adopted and improved the microfluidic device proposed by Moraes *et al.*[22, 24] to be equipped with an array of cell compression units. Our device contained a 5×5 array of alginate-chondrocyte constructs that

Author Manuscript Author Manuscript Author Manuscript Author Manuscript

were compressed by a PDMS membrane or balloon (Layer 2) driven by pressurized air (Fig. 1b and d). Different magnitudes of compressive strain (14–34%) on alginate columns were generated within a single device using PDMS balloons of different sizes (1.2–2.0 mm in diameter) inflated with the same air pressure (14 kPa in these experiments). Under these static compression conditions, chondrocyte strain was 7–19% as a function of PDMS balloon diameter. Cell viability was 80% and 85% for uncompressed and dynamically compressed chondrocytes, respectively. Therefore, the developed device can compress chondrocytes with different magnitudes simultaneously with negligible effect on cell viability, and enable time- and cost-efficient study of mechanobiological behaviors of chondrocytes.

## Materials and Methods

### Microfluidic unit

The microfluidic part of the device consisted of two layers (Layer 1 and 2) of PDMS [Sylgard 184, Dow Corning, Midland, MI; 10:1 (weight ratio between prepolymer and curing agent)] on a glass slide (Glass plate 1) and a tubing block (Fig. 1a). The detailed fabrication procedure is shown in the Supplementary Information (SI).

Briefly, the SU-8 master mold for Layer 1 was fabricated on a clean glass slide (50.8 mm × 76.2 mm × 1.2 mm, Fisher Scientific, Hampton, NH) using SU-8 (MicroChem Corp. Westborough, MA). A thin layer of SU-8 5 was formed on the glass slide for enhanced adhesion of SU-8 channel patterns on the glass. Then, microchannel geometry was fabricated on the seed layer using SU-8 100 and a photomask (25,400 dpi; CAD/Art Services, Bandon, OR) based on the photolithography technique (Fig. S1).[25] The channel height on the mold was about 90 μm (87.1 ± 1.3 μm, $n = 5$ points on a single mold) which was measured with a three-dimensional (3D) laser scanning microscope (VK-X200, Keyence, Osaka, Japan).

Layer 1 was prepared using the sandwich molding method[26] to prevent PDMS shrinkage.[27] The SU-8 master mold was coated with (Tridecafluoro-1, 1, 2, 2-Tetrahydrooctyl)-1-Trichlorosilane (T2492-KG, United Chemical Technologies, Bristol, PA) for easy release of PDMS from the mold.[28] Uncured PDMS was sandwiched between a transparency film (HP Transparencies for LaserJets, C2934A) and the mold (Fig. S1a), and it was cured at 80 °C for 6 hours (or overnight). Cured Layer 1 was then bonded on Glass plate 1 via plasma bonding. After additional baking at 80 °C for 30 min, the transparency film was removed.

For Layer 2, PDMS was spin coated on a transparency film at 1,000 rpm for 1 minute using a spin coater (WS-650MZ-23NPPB, Laurell Technologies Corporation, North Wales, PA) to obtain 60 μm in thickness (Fig. S1b and S2), and then it was partially cured at 80 °C for 20–30 minutes. Layer 1 and 2 were bonded via plasma bonding and baked at 80 °C overnight. After cooling down the device, the transparency film was removed from Layer 2, and the tubing block was attached to Layer 2 using plasma bonding.

Author Manuscript Author Manuscript Author Manuscript Author Manuscript

### Alginate-chondrocyte constructs

An array of alginate-chondrocyte constructs was fabricated using the alginate gel micropatterning method (Fig. S1c).[29, 30] First, an aluminium mold was machined with the same dimension and geometry of the gel array. Second, an agarose gel mold with a 5 × 5 array of holes was prepared by casting 5% (w/v) agarose gel (SeaKem LE Agarose, Lonza, Basel, Switzerland) containing 200 mM $CaCl_2$ on the aluminium mold. Third, 1.5% (w/v) alginate gel solution (Pronova UP MVG, FMC Corporation, Philadelphia, PA) was mixed with 5 mg/ml Sulfo-NHS (Thermo Fisher Scientific, Waltham, MA), 10 mg/ml 1-ethyl-3-(3-dimethylaminopropyl)carbodiimide hydrochloride (EDC, Thermo Fisher Scientific, Waltham, MA) and chondrocytes (or fluorescent beads). Fourth, 170 μl of the alginate gel solution was placed on an aminopropyltriethoxysilane (APTES)-coated Glass plate 2 (see SI). Last, the alginate gel solution was covered with the agarose gel mold for 3 minutes. After detaching the agarose gel mold from the alginate gel, the formed array of alginate gel constructs was placed in the cross linking solution (50 mM $CaCl_2$ + 140 mM NaCl) for 1 minute for further polymerization. The dimensions of each construct were 0.81 ± 0.02 mm in diameter and 0.96 ± 0.02 mm in height ($n$ = 85 gel constructs).

### Device assembly and operation

Four ~1 mm-thick PDMS spacers were located on the four corners of Glass plate 2 where the alginate gel constructs were attached. Then, Glass plate 2 was placed on the microfluidic part of the device with the gel constructs facing toward the PDMS balloons (Fig. 1 and S1d). The entire device was fastened with 3D printed clamps for easy disassembly.

The assembled cell compression device was connected to a solenoid valve (S10MM-30–12-3, Pneumadyne, Plymouth, MN) and an air pump (SP 500 EC-LC, Schwarzer Precision, Essen, Germany) via silicon tubing. The device was actuated by pressurized air (14 kPa, gauge pressure) from the air pump that was connected to the device via a solenoid vale. For static compression, the solenoid valve was fully opened to supply constant air pressure. For dynamic compression, a function generator (SDG1025, Siglent, China) connected to the solenoid valve regulated the solenoid valve with a square wave.

### Compression capability characterization

The compression capability of the cell compression device depends on the diameter and air pressure of the PDMS balloons of Layer 2. Thus, we characterized the deformation of the PDMS balloons, alginate gels and chondrocytes as a function of the balloon diameter with the fixed air pressure of 14 kPa, which was the minimum gauge pressure of the air pump.

The center height ($h$) of the expanded PDMS balloons was measured using surface imaging without any samples on them (Fig. 2a). The PDMS balloons were imaged using the 3D laser scanning microscope, and their maximum height was measured by VK analyser software (Keyence, Osaka, Japan). The measured maximum height was equated to be the center height assuming axisymmetric expansion. For better imaging, the top surface of the PDMS balloons was made opaque by using a transparency film silanized with (Tridecafluoro-1, 1, 2, 2-Tetrahydrooctyl)-1-Trichlorosilane for Layer 2 fabrication.

Author Manuscript Author Manuscript Author Manuscript Author Manuscript

Deformation of alginate gel constructs and chondrocytes was measured using a confocal fluorescence microscope (LSM 800, Carl Zeiss AG, Oberkochen, Germany) at 10× and 20×, respectively. For gel deformation measurement, 0.3% (v/v) of 1.0 μm-diameter fluorescent beads (542/612 nm, Fluoro-Max Red Aqueous Fluorescent Particles, Thermo Fisher Scientific, Waltham, MA) were mixed with 1.5% alginate gel.

To measure cell deformation under compressive strain, chondrocytes were isolated from the growth plate cartilage of neonatal mice by digestion in 0.25% collagenase (Sigma-Aldrich, St. Louis, MO) for 3 hours at 37 °C, and ECM material was removed from the cell suspension by gravity. Chondrocytes were labelled by 2 μM calcein AM (Invitrogen) diluted in Dulbecco's Modified Eagle's medium (DMEM) containing 10% Fetal Bovine Serum (FBS) for 30 minutes. Fluorescent labelled chondrocytes were pelleted by centrifugation for 5 minutes at 125*g* and then suspended in sterile-filtered 1.5% alginate gel at a density of $8 \times 10^6$ cells/mL.

Arrays of alginate gel constructs containing either marker beads or chondrocytes were assembled in the microfluidic cell compression device as previously described and the space between Layer 2 and Glass plate 2 was filled with a culture medium (alpha-MEM supplemented with ITS+3, 1mM Beta-glycerophosphate, antioxidant, non-essential amino acids, ascorbic acid, sodium pyruvate, glutamine, penicillin and streptomycin[31]). Volumetric data of either alginate gel columns containing labelled beads or chondrocytes were obtained before compression and during compression using confocal microscopy with nominal *z*-step sizes of 10 μm and 0.5 μm, respectively (respective optical section thickness = 13.2 μm and 5 μm). The actual *z*-step size was calibrated to be 13 μm and 0.68 μm, respectively.[32]

The height of alginate gel columns and chondrocytes was measured by image processing with MATLAB (MathWorks, Natick, MA) (Fig. S4; see SI).[32] Their compressive (or axial) strain was calculated by dividing the measured height change by the initial sample height. With the same image processing code, the diameter of chondrocytes was measured by averaging the cell widths in *x* and *y* directions at the center of each cell under the assumption that the cells were axisymmetric. In contrast, the diameter of alginate gel constructs was measured differently due to sparse distribution of fluorescent beads in the gel. On the *xy* image at the gel center, 3 beads on the gel boundary were selected for 3 points circular fitting to determine the gel diameter. The lateral (or transversal) strain of the samples was calculated as a ratio of the diameter change due to compression to the initial sample diameter.

## Finite element method simulation

Finite element method (FEM)-based simulations using Abaqus (Dassault Systèmes, Vélizy-Villacoublay, France) were conducted to predict and analyse PDMS balloon deformation. A two-dimensional (2D) axisymmetric FEM model consisting of 1350 quadrilateral elements was created (Fig. S5), and the axisymmetric and fixed boundary conditions were applied to the axis of symmetry and bottom of the model, respectively. Pressure of 14 kPa was applied at the inner surface of the PDMS balloon (Fig. S5b). Young's modulus of the PDMS ($E_{PDMS}$) was measured to be 1.86 MPa by the tensile test (see SI). Poisson's ratio ($\nu$) of PDMS was assumed as 0.49.[33]

Author Manuscript Author Manuscript Author Manuscript Author Manuscript

### Chondrocyte viability test

Viability of chondrocytes in alginate-chondrocyte constructs was assessed via the live/dead cell viability kit (Invitrogen, Carlsbad, CA). Alginate-chondrocyte constructs were subjected to dynamic compression (14 kPa, 1 Hz) for 1 hour, whereas control groups were in the identical condition without compression. Both constructs were cultured out of the device for 24 hours and then incubated in Phosphate-buffered saline (PBS) containing 2 μM calcein AM and 4 μM ethidium homodimer-1 (EthD-1) for 0.5 hour in the dark room. The incubated constructs were washed 3 times in PBS for 5 minutes per each.

The constructs were imaged using an inverted microscope (DMI6000B, Leica microsystems, Wetzlar, Germany) to measure fluorescence in the green (live cells) and red (dead cells) channels to count the number of live and dead cells, respectively. Percent viability (the number of live cells divided by the number of total cells) of chondrocytes was quantified by counting the number of live and dead cells in the resulting images. The “make binary” and “analyse objects” functions in ImageJ[34] were used for image analysis.

### Statistical analysis

All values were reported as mean ($m$) ± standard deviation ($\sigma$). To determine if calculated mean values between multiple groups were significantly different, one-way analysis of variance (ANOVA) and Tukey’s multiple comparison test were used. For comparisons of mean values between two groups, Student’s $t$-test was used. 0.05 was selected as a significance level in statistical analysis.

## Results

Although the described microfluidic cell compression device was developed to dynamically compress alginate-chondrocyte constructs in a controlled manner, the initial characterization of performance was conducted under static compression except for the final cell viability test. Static compression conditions were used because volumetric imaging using confocal microscopy is a slow process (e.g., minutes long) that cannot generate the required high-resolution images for quantitative analysis when cells are dynamically compressed. Therefore, our approach was to characterize the device by measuring the compressive strain of chondrocytes under static compression and then to use the device for dynamic compressive stimulation of the cells. Our results show that the developed device generated different magnitudes of compressive strain on alginate-chondrocyte constructs (Table 1) and that cells could survive dynamic compression.

### PDMS balloon expansion

To quantify the compression capability of the developed device, we first imaged the surface topography of the inflated PDMS balloons (Fig. 2a). The center height ($h$) of the inflated balloon was characterized as a function of the balloon diameter ($D$) with the fixed air pressure of 14 kPa (Fig. 2b). On a single device, the standard deviation of $h$ was less than 3.4% with respect to the mean value of $h$ ($\sigma_h/m_h < 3.4\%$) among the PDMS balloons of the same diameter (Fig. 2b). Thus, the PDMS balloons on the single device were inflated uniformly when their sizes were same. Also, $h$ increased with $D$; the $m_h$ values of the

Author Manuscript Author Manuscript Author Manuscript Author Manuscript

examined device were 167.2 ± 3.3, 214.3 ± 7.4, 250.9 ± 2.8, 291.0 ± 2.5 and 342 ± 4.9 μm for $D$ of 1.2, 1.4, 1.6, 1.8 and 2.0 mm, respectively (Device 1 in Table S1). It was found that all $m_h$ values were significantly different as $D$ increased ($p < 0.05$). Also, $h$ increased around 45 μm per 0.2 mm increase in $D$, and this information can be used for tuning the performance of the device. These results demonstrate that balloons of the same size display consistent compression characteristics and that compressive strain is predictable for a known balloon diameter.

To confirm the repeatability of the fabrication method, we tested two more devices and determined the variation among the three devices using the relative standard deviation of $h$ ($RSD_h$), a ratio of the standard deviation of $m_h$ to the average of $m_h$. The maximum $RSD_h$ of 6.9% was found with the smallest PDMS balloons, and $RSD_h$ decreased with $D$ to the minimum value of 2.2% (see Table S1). Also, all three devices showed that the larger the PDMS balloon was, the more it protruded, as expected (Fig. 2c and Table 1).

Although the measurements varied more between devices than within a device, average measurements across three devices showed similar consistent values for a given balloon size, as well as the same strong relationship between $h$ and $D$ as observed in a single device. Therefore, the fabrication method is repeatable because it produced similarly operating devices.

## FEM simulation of PDMS balloon expansion

The deformation of PDMS balloons was simulated by the FEM numerical model to validate the experimental measurements and to analyse and predict the deformation of the PDMS balloon for possible changes in the device design (Fig. 3a and S5). For efficient simulations, the optimum element number of the model was determined by calculating $h$ as a function of the number of elements with $D = 2$ mm (Fig. S6); $h$ converged as the number of elements increased, and it became nearly constant when the element of number was 1,350. Thus, the FEM model of 1,350 elements was used.

The mean PDMS balloon profiles from 3D imaging and FEM simulation are compared in Fig. 3b. The mean balloon profile was obtained by averaging balloon profiles with respect to the location of maximum height of individual balloon. Overall, the simulated profiles were close to the measured profiles although 3D images contained errors near the center and boundary of the balloon (Fig. 2a and Fig. 3b). Those errors might be caused because the whitish coating on the balloon for imaging became nonuniform as the balloon expanded. Figure 2c shows that the $h$ values obtained by the two methods are in good agreement because their relative errors ($|h_{exp}-h_{FEM}|/h_{FEM}$) were 0.2-3.2%. Therefore, both the imaging-based $h$ measurements and the FEM model were validated.

The FEM simulation enabled examining the deformation of the PDMS balloon in more detail. When the balloon was inflated, stress concentration occurred where Layer 2 and the air chamber met (Fig. 3a). Accordingly, the maximum stress and strain were found at the said location on PDMS balloons of different diameters (Table S2). Therefore, the PDMS balloon is expected to rupture along its perimeter if too high pressure is applied. Also, the simulation showed that the PDMS balloon got thinner during expansion as expected. The

Author Manuscript Author Manuscript Author Manuscript Author Manuscript

maximum decrease in the balloon thickness occurred at the balloon center (Table S2), while the thickness change was minimal along the balloon perimeter. Therefore, the FEM model can be used to predict the expansion of PDMS balloons of the cell compression device if the device design needs to be changed.

## Alginate gel deformation

Figure 4a shows the 5 × 5 array of alginate gel constructs (~0.8 mm in diameter and ~1 mm in height) cast on Glass plate 2. To measure the alginate gel deformation due to static compression, fluorescent beads were included in the gel instead of chondrocytes, and *z*-stack images of gel constructs was obtained using confocal microscopy. Because the embedded beads could affect the mechanical property of the gel, a relatively low number of the beads were introduced to the gel, which made it difficult to visualize a vertical cross-section of the gel. Instead, the obtained *z*-stack was projected to the *xz* plane as shown in Fig. 4b. This example shows that the height of the gel on the largest PDMS balloon ($D = 2.0$ mm) decreased from 1,001 μm to 663 μm under compression. Therefore, the gel was compressed by 33.8% due to the expanded PDMS balloon.

The compressive strain of the gel construct ($\varepsilon_{gel}$) is the gel height change divided by the initial gel height. Figure 4c shows how $\varepsilon_{gel}$ changed with $D$. As expected from Fig. 2c, the alginate gel was compressed more on a larger PDMS balloon (Table 1). The observed differences in $\varepsilon_{gel}$ are significant with respect to the change in $D$ ($p < 0.05$), and the amount of $\varepsilon_{gel}$ increased approximately 5% per 0.2 mm increment of $D$. In contrast to the gel height, the diameter of the gel constructs was barely changed by compression because the resultant lateral strain was smaller than 4%.

Because the alginate gel is much softer than PDMS ($E_{gel}$ = 40.7 kPa and $E_{PDMS}$ = 1.86 MPa, see Fig. S3), the gel height change ($\Delta h_{gel}$) was expected to be close to the central height ($h$) of the PDMS balloon, i.e., $\Delta h_{gel} \approx h$. As shown in the inset of Fig. 4b, $\Delta h_{gel}$ was smaller than $h$ for the smallest balloon, but the difference decreased with $D$. For the largest balloon, $\Delta h_{gel}$ was 338 μm, close to the $m_h$ value (335 μm). This comparison suggests that the compression capability of the smaller PDMS balloons was affected by the gel, and it validates the imaging-based measurement of gel height.

## Chondrocyte deformation

Having demonstrated consistent and predictable deformation of materials in these devices, we next determined the resulting compressive strain in chondrocytes embedded in these gels. Compressive strain of chondrocytes was determined under static compression conditions by confocal imaging of a 613 μm × 613 μm × 40–55 μm ($x \times y \times z$) volume (around gel center) that was 300–400 μm from the gel base as shown in Fig. 5a. Figure 1d shows representative chondrocyte images before and under compression on the largest PDMS balloon ($D = 2.0$ mm). Because the cell height decreased from 17.0 μm to 14.3 μm, the resultant compressive strain of the chondrocyte ($\varepsilon_{cell}$) was 16%, which is lower than that of the gel (34%). The mean strain of chondrocytes is approximately 50% of the gel strain (Table 1, Fig. S7). This difference may be due to different mechanical properties (e.g., viscoelastic properties) of the alginate gel and chondrocyte.[35]

Author Manuscript Author Manuscript Author Manuscript Author Manuscript

Figure 5b shows the distribution of the measured $\varepsilon_{cell}$ values ($n$ = 35-47 cells for each balloon size), and the mean $\varepsilon_{cell}$ values are shown in Table 1. The resulted $\varepsilon_{cell}$ range (7-19%) is similar to that of growth plate chondrocytes caused by physiological stress condition (7-23%).[36] There were no significant differences in $\varepsilon_{cell}$ between adjacent PDMS balloons of different diameters (e.g., for 1.2 mm vs 1.4 mm, 1.4 mm vs 1.6 mm, 1.6 mm vs 1.8 mm, and 1.8 mm vs 2.0 mm, $p > 0.05$). However, the compressive strains were significantly different for all other pairs ($p < 0.05$). Although the standard deviation of $\varepsilon_{cell}$ is large, up to 80 % of mean value, $\varepsilon_{cell}$ seems proportional $D$ (Fig. 5b). It was also noticed that the mean and median values of $\varepsilon_{cell}$ were close, which suggests relatively symmetric distribution, even with longer positive tails. In comparison to the cell height, the diameter of the cells showed smaller changes due to compression. The measured lateral strain values were 1.7 ± 3.4, 2.3 ± 3.0, 3.8 ± 3.1, 3.7 ± 2.6 and 4.9 ± 2.6% for the balloon diameter of 1.2, 1.4, 1.6, 1.8 and 2.0 mm, respectively. Therefore, the developed microfluidic cell compression device could apply compression of different magnitudes to chondrocytes on a single device.

### Viability of chondrocytes under dynamic compression

To determine whether the developed device was suitable for applying dynamic compression to chondrocytes, we assessed cell viability with and without dynamic compression using three different devices per each condition. Live/Dead assay of cultured chondrocytes showed an average of 80.7% viability in the non-compressed devices (Fig. 6). When dynamic compression was applied, chondrocyte viability increased to an average of 85.6%, but this change was not significant ($p > 0.05$). This result suggests that dynamic compression on chondrocytes in the device had negligible effect on the survival of chondrocytes. In contrast to dynamic compression, static compression resulted in cell viability of 58.6%. According to the previsous research,[37, 38] solute transport is enhanced in the porous media under dynamic compression, which may be related to nutrient transport. Thus, alginate-chondrocyte constructs under dynamic compression may promote nutrient transport, which resulted in better cell viability under dynamic compression than under static compression.

## Discussion

Not only chemical signals but also mechanical signals drive cellular functions, and collective effects of mechanobiology of cells create a bigger impact on the organ level functions. Thus, cell mechanobiology studies will provide valuable insights to understand the unknown mechanism of developmental biology, pathogenesis, and maintenance of human health. For example, examining the effects of compressive stress on chondrocyte mechanobiology is critical for understanding bone growth and bone disease development such as infant musculoskeletal deformities[5] and osteoarthritis[39]. Because different compressive stress conditions trigger distinct cell responses, it is imperative to test multiple stress conditions in mechanobiology studies. However, conventional compression devices are not designed to simultaneously test different compressive stress conditions.

We adopted and improved the idea of the microfluidic device proposed by Moraes *et al.*[22, 27] to generate distinct levels of compressive stress on a single platform to increase the

Author Manuscript Author Manuscript Author Manuscript Author Manuscript

throughput for studies of chondrocyte mechanobiology. To allow rapid isolation of mechanically stimulated cells for post-stimulation biomechanical and biochemical analysis, we incorporated a reversible sealing process and used alginate hydrogel.

Alginate is rapidly polymerized in the presence of calcium ions ($Ca^{2+}$) and depolymerised in low concentrations of calcium chelators. By contrast, it is more difficult to harvest cells from photopolymerized hydrogels, and there are potential concerns about the photopolymerization process. In particular, ultraviolet (UV) photopolymerization of hydrogel-cell constructs may need more rigorous characterization of the effects of the photo initiator and UV exposure parameters on cell viability.[40] Although gelation conditions for alginate hydrogel are considered gentle on cells, the effect of $Ca^{2+}$ concentration on cell viability depends on the cell type.[29, 30, 41, 42] Therefore, optimal $Ca^{2+}$ concentration and crosslinking time should be empirically determined for different experimental designs.

It needs to be noticed that the used alginate gel is much softer than native growth plate cartilage: the $E$ of the alginate gel and growth plate cartilage are 40.7 kPa (Fig. S3) and 0.3–1.1 MPa[5], respectively. However, the chondrocytes in the alginate gel culture behave like those in native tissue samples.[31] Therefore, alginate gel is regarded as one of the ideal materials for *in vitro* study of chondrocyte mechanobiology.

One downside of using alginate gel is that the final shape of cross-linked alginate gel is usually limited to spherical shape because the gel solution is immediately cross-linked upon contact with $Ca^{2+}$. For the current device, the cylindrical alginate gel columns were fabricated using the gel patterning methods (Fig. 4a and S1c).[29, 30, 43, 44] The method enables manipulating the gel shape by slowing the discharge of $Ca^{2+}$ from the agarose gel mold to the alginate gel solution. However, the method may not be appropriate for large alginate gels due to longer gelation time.

The cell compression capability of the developed device depends on the expansion of its PDMS balloons, and we evaluated the balloon expansion in terms of the center height ($h$) and diameter ($D$) of the inflated balloons using 3D surface topography imaging and FEM simulation. Similarity in the results of the two methods demonstrated that the PDMS balloons behaved as expected: $h$ increased with $D$ (Fig. 2c). Moreover, the gel did not significantly resist compression by the PDMS balloon (Fig. 4c inset). Therefore, predictable device modification would be possible with FEM simulation.

The expansion of the PDMS balloon was controlled by the diameter of the balloon in our application. Alternatively, the balloon expansion could be regulated by controlling the applied air pressure and the thickness of the balloon, as shown by the following approximate analytical model for clamped thin film deformation[45, 46]:

$$h = \left( \frac{3P(D/2)^4(1-\nu)}{E_{PDMS}(7-\nu)^t} \right)^{\frac{1}{3}}, \quad (1)$$

Author Manuscript Author Manuscript Author Manuscript Author Manuscript

where $P$ is air pressure, and $t$ is the PDMS balloon thickness. Eqn (1) shows that $h$ increases with increase in $P$ and $D$ and decrease in $t$. However, eqn (1) estimated lower $h$ values than the measurement and simulation did although the approximate model showed a similar trend in $h$ increasing with $D$ (Fig. 2c). This is because eqn (1) is based on the assumption of $h << D/2$, which the developed device does not satisfy.

Also, the approximate model can explain the observed variation among the fabricated devices. The thickness and elasticity of spin-coated PDMS for Layer 2 could have variation (see SI and Fig. S2). The uncertainty in $h$ is found using eqn (1) to be

$$\frac{\sigma_h}{m_h} = \sqrt{\left[-\frac{1}{3}\cdot\frac{\sigma_t}{m_t}\right]^2 + \left[-\frac{1}{3}\cdot\frac{\sigma_{E_{PDMS}}}{m_{E_{PDMS}}}\right]^2}, \quad (2)$$

where $\sigma_t/m_t$ (1.7 μm/61.8 μm) and $\sigma_{EPDMS}/m_{EPDMS}$ (0.22 MPa/1.86 MPa) are relative error in $t$ and $E_{PDMS}$ (see SI). Thus, uncertainty of $h$ was calculated to be ~4%, which is close to experimental deviation of $h$ (2.2-6.9%).

The objective of our microfluidic cell compression device is to estimate the effects of dynamic compression on chondrocyte mechanobiology. However, the deformation of alginate gel was measured under the static compression condition (Fig. 4c) because imaging gels and cells under dynamic compression was challenging with the conventional confocal microscopy. Because alginate gel is known to undergo permanent deformation under static mechanical loading[47], we tested the effects of static (14 kPa, 1 hr) and dynamic compression (14 kPa, 1 Hz, 1 hr) on the permanent deformation of alginate gel in the device (Fig. S8). While the static compression resulted in permanent deformation of 9-30%, the dynamic compression induced permanent deformation of 0.5–6%. Therefore, the permanent deformation of alginate gel appears negligible under dynamic compression, and the proposed device can be used for cell dynamic compression studies.

Similar to the alginate gel, the deformation of chondrocytes seemed to be proportional to the diameter of the PDMS balloon (Fig. 5b). The compressive strain of chondrocytes ($\varepsilon_{\text{cell}}$) increased ~2.9% per 0.2 mm increment of the balloon diameter. However, the standard deviation of $\varepsilon_{\text{cell}}$ was 34-80% of the mean values. The wide range of compressive strain on chondrocytes may be a result of natural variability among chondrocytes. This might suggest chondrocytes show highly heterogeneous behaviors as response to mechanical stimulation. This mechanobiology of chondrocytes is what our device was designed to test, and the observed variable compressive strain of chondrocytes shows the importance of single cell studies. Most studies examine average cell responses for a population. However, our device enables us to study both average and individual cell responses (Fig. 5b). For instance, the device can be mounted on a microscope to image individual cells that could include fluorescence-based reporters for biological processes, and cells can be easily harvested from the hydrogel for downstream analysis by single cell sequencing methods.

Author Manuscript Author Manuscript Author Manuscript Author Manuscript

It is also possible to fabricate and use several chips, each with a different balloon size, for various biological assays. However, the chip with multiple compression levels would be beneficial for real-time imaging of live cells under the multiple compression conditions without changing the chips during optical imaging. This would enable us to examine the chondrocyte behavior quickly so that it will be easy to determine the optimum experimental conditions. For practical application of the device for other types of hydrogels and cells, the calibration of the device will be needed because the level of cell deformation in response to PDMS balloon expansion will be affected by the mechanical property (e.g., elasticity) of surrounding hydrogels and cells. It may limit the types of hydrogels applied in the device.

## Conclusions

Studying the effects of compressive stress on growth plate chondrocytes' function is critical for understanding the underlying mechanism of bone growth. To mechanically stimulate chondrocytes, conventional macroscopic compression devices have been widely used. However, the conventional approaches have limited productivity to examine the mechanobiological behaviors of chondrocytes. Thus, we proposed the pneumatic microfluidic cell compression device to enhance the efficiency of chondrocytes' mechanobiology study.

The proposed device generated multiple magnitudes of compressive stress on a single platform for high-throughput test of chondrocytes' response induced by compressive stress conditions. We characterized the device performance with imaging technique, mechanical testing, FEM simulations and cell viability test. Our data show that the amount of cell compression can be manipulated by controlling the size of the PDMS balloon of the device, and the developed device had negligible effect on cell viability. Therefore, the proposed device can enable time- and cost-efficient mechanobiological study of chondrocytes, and it can be a valuable tool for other cell types.

## Supplementary Material

Refer to Web version on PubMed Central for supplementary material.

## Acknowledgements

We thank Dr. Moraes for his assistance for device design and fabrication. This study was supported by Bioengineering for Human Health grant from the University of Nebraska-Lincoln (UNL) and the University of Nebraska Medical Center (UNMC), and grant AR070242 from the NIH/NIAMS. 3D surface imaging was performed at the NanoEngineering Research Core Facility (part of the Nebraska Nanoscale Facility), which is partially funded from the Nebraska Research Initiative.

## Notes and references

1. Eyckmans J, Boudou T, Yu X and Christopher S. Chen, Dev. Cell, 2011, 21, 35–47. [PubMed: 21763607]
2. Smith SM and Heer M, Nutrition, 2002, 18, 849–852. [PubMed: 12361777]
3. Alberty A, Peltonen J and Ritsilä V, Acta Orthop. Scand, 1993, 64, 449–455. [PubMed: 8213126]
4. Robling AG, Duijvelaar KM, Geevers JV, Ohashi N and Turner CH, Bone, 2001, 29, 105–113. [PubMed: 11502470]

Author Manuscript Author Manuscript Author Manuscript Author Manuscript


5. Villemure I and Stokes IAF, J. Biomech, 2009, 42, 1793–1803. [PubMed: 19540500]
6. Jacobs CR, Huang H and Kwon RY, Introduction to cell mechanics and mechanobiology, Garland Science, 2013.
7. Kim D-H, Wong PK, Park J, Levchenko A and Sun Y, Annu. Rev. Biomed. Eng, 2009, 11, 203–233. [PubMed: 19400708]
8. Guilak F, Biomech J., 1995, 28, 1529–1541.
9. Knight MM, Ghori SA, Lee DA and Bader DL, Med. Eng. Phys, 1998, 20, 684–688. [PubMed: 10098613]
10. Kisiday JD, Jin M, DiMicco MA, Kurz B and Grodzinsky AJ, J. Biomech, 2004, 37, 595–604. [PubMed: 15046988]
11. Sergerie K, Lacoursière M-O, Lévesque M and Villemure I, J. Biomech, 2009, 42, 510–516. [PubMed: 19185303]
12. Amini S, Veilleux D and Villemure I, J. Biomech, 2010, 43, 2582–2588. [PubMed: 20627250]
13. Sergerie K, Parent S, Beauchemin P-F, Londoño I, Moldovan F and Villemure I, J. Orthop. Res, 2011, 29, 473–480. [PubMed: 21337387]
14. Bougault C, Paumier A, Aubert-Foucher E and Mallein-Gerin F, BMC Biotechnol, 2008, 8, 71. [PubMed: 18793425]
15. Lu H, Koo LY, Wang WM, Lauffenburger DA, Griffith LG and Jensen KF, Anal. Chem, 2004, 76, 5257–5264. [PubMed: 15362881]
16. Malek AM and Izumo S, J. Cell Sci, 1996, 109, 713–726. [PubMed: 8718663]
17. Paguirigan AL and Beebe DJ, BioEssays, 2008, 30, 811–821. [PubMed: 18693260]
18. García-Cardeña G, Comander J, Anderson KR, Blackman BR and Gimbrone MA, Proc. Natl. Acad. Sci. U.S.A, 2001, 98, 4478–4485. [PubMed: 11296290]
19. Birukov KG, Birukova AA, Dudek SM, Verin AD, Crow MT, Zhan X, DePaola N and Garcia JGN, Am. J. Respir. Cell Mol. Biol, 2002, 26, 453–464. [PubMed: 11919082]
20. Huh D, Matthews BD, Mammoto A, Montoya-Zavala M, Hsin HY and Ingber DE, Science, 2010, 328, 1662–1668. [PubMed: 20576885]
21. Moraes C, Chen J-H, Sun Y and Simmons CA, Lab Chip, 2010, 10, 227–234. [PubMed: 20066251]
22. Moraes C, Wang G, Sun Y and Simmons CA, Biomaterials, 2010, 31, 577–584. [PubMed: 19819010]
23. Sundararaghavan HG, Monteiro GA, Firestein BL and Shreiber DI, Biotechnol. Bioeng, 2009, 102, 632–643. [PubMed: 18767187]
24. Moraes C, Zhao R, Likhitpanichkul M, Simmons C, and Y A. Sun, J. Micromech. Microeng, 2011, 21, 054014.
25. Lorenz H, Despont M, Fahrni N, Brugger J, Vettiger P and Renaud P, Sensors and Actuators A: Physical, 1998, 64, 33–39.
26. Jo BH, Lerberghe LMV, Motsegood KM and Beebe DJ, J. Microelectromech. Syst, 2000, 9, 76–81.
27. Moraes C, Sun Y and Simmons CA, J. Micromech. Microeng, 2009, 19, 065015.
28. Anderson JR, Chiu DT, Jackman RJ, Cherniavskaya O, McDonald JC, Wu H, Whitesides SH and Whitesides GM, Anal. Chem, 2000, 72, 3158–3164. [PubMed: 10939381]
29. Agarwal A, Farouz Y, Nesmith AP, Deravi LF, McCain ML and Parker KK, Adv. Funct. Mater, 2013, 23, 3738–3746. [PubMed: 26213529]
30. Talei Franzesi G, Ni B, Ling Y and Khademhosseini A, J. Am. Chem. Soc, 2006, 128, 15064–15065. [PubMed: 17117838]
31. Erickson AG, Laughlin TD, Romereim SM, Sargus-Patino CN, Pannier AK and Dudley AT, Tissue Eng. Part A, 2017.
32. Lee D, Rahman MM, Zhou Y and Ryu S, Langmuir, 2015, 31, 9684–9693. [PubMed: 26270154]
33. Park J, Kim IC, Baek J, Cha M, Kim J, Park S, Lee J and Kim B, Lab Chip, 2007, 7, 1367–1370. [PubMed: 17896023]
34. Schneider CA, W. S. Rasband and K. W. Eliceiri, Nat. Methods, 2012, 9, 671–675. [PubMed: 22930834]

Author Manuscript Author Manuscript Author Manuscript Author Manuscript


35. Knight MM, van J de Breevaart Bravenboer, D. A. Lee, G. J. V. M. van Osch, H. Weinans and D. L. Bader, Biochim. Biophys. Acta*, Gen. Subj.*, 2002, 1570, 1–8. [PubMed: 11960682]
36. Gao J, Roan E and Williams JL, PLoS ONE, 2015, 10, e0124862. [PubMed: 25885547]
37. Albro MB, Chahine NO, Li R, Yeager K, Hung CT and Ateshian GA, J. Biomech, 2008, 41, 3152–3157. [PubMed: 18922531]
38. Mauck RL, Hung CT and Ateshian GA, J. Biomech. Eng, 2003, 125, 602–614. [PubMed: 14618919]
39. Loeser RF, Goldring SR, Scanzello CR and Goldring MB, Arthritis Rheum, 2012, 64, 1697–1707. [PubMed: 22392533]
40. Bryant SJ, Nuttelman CR and Anseth KS, J. Biomater. Sci. Polym. Ed, 2000, 11, 439–457. [PubMed: 10896041]
41. Maeno S, Niki Y, Matsumoto H, Morioka H, Yatabe T, Funayama A, Toyama Y, Taguchi T and Tanaka J, Biomaterials, 2005, 26, 4847–4855. [PubMed: 15763264]
42. Utech S, Prodanovic R, Mao AS, Ostafe R, Mooney DJ and Weitz DA, Adv. Healthc. Mater, 2015, 4, 1628–1633. [PubMed: 26039892]
43. Khademhosseini A, Eng G, Yeh J, Fukuda J, Blumling J, Langer R and Burdick JA, J. Biomed. Mater. Res. A, 2006, 79A, 522–532.
44. Yeh J, Ling Y, Karp JM, Gantz J, Chandawarkar A, Eng G, Blumling Iii J, Langer R and Khademhosseini A, Biomaterials, 2006, 27, 5391–5398. [PubMed: 16828863]
45. Lin P, Massachusetts Institute of Technology, 1990.
46. Small MK and Nix WD, J. Mater. Res, 1992, 7, 1553–1563.
47. Mancini M, Moresi M and Rancini R, J. Texture Stud, 1999, 30, 639–657.

Author Manuscript Author Manuscript Author Manuscript Author Manuscript

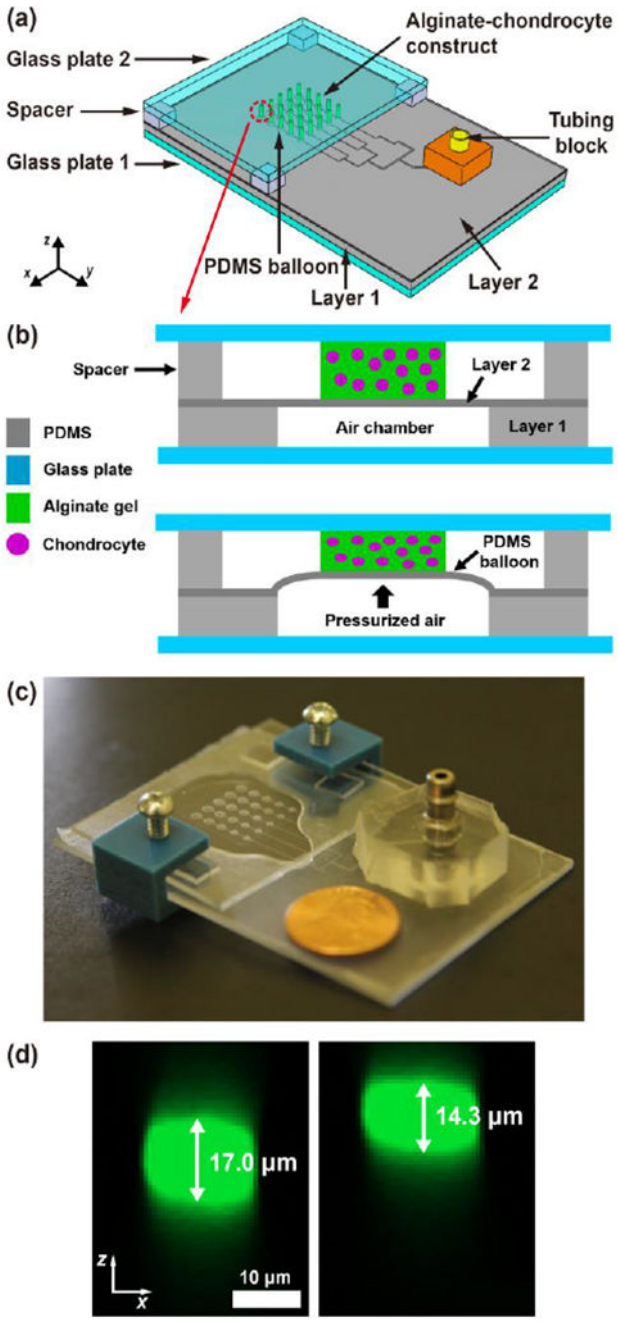


**Fig. 1.**

Pneumatic microfluidic cell compression device. (a) The device has a 5×5 array of PDMS balloons with different diameters ($D$ = 1.2, 1.4, 1.6, 1.8 and 2.0 mm), and alginate-chondrocyte constructs are located on the PDMS balloons. (b) The constructs are compressed by the balloon inflated by pressurized air. (c) Image of an actual device (coin diameter = 19 mm). (d) Cross-sectional images of a chondrocyte before (left) and under (right) compression show that the cell was compressed by the device with a static compression (cell compressive strain, $\varepsilon_{cell}$ = 16%).

Author Manuscript Author Manuscript Author Manuscript Author Manuscript

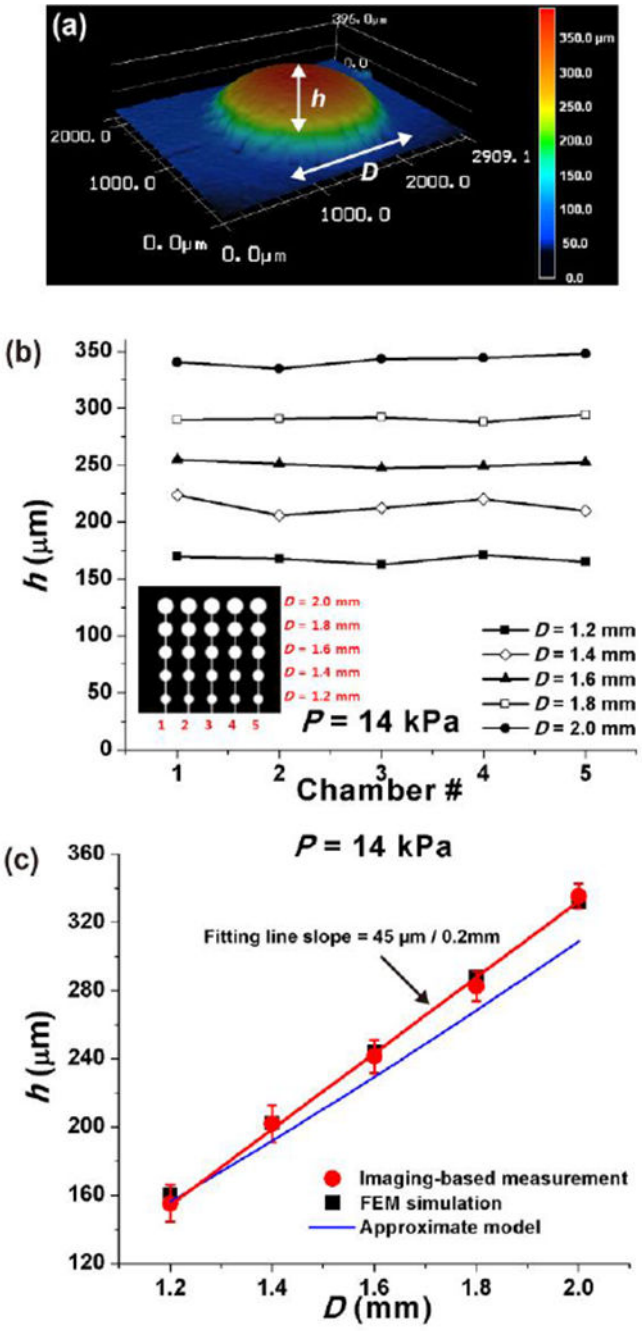


**Fig. 2.**

Deformation of the PDMS balloons (Layer 2) inflated by pressurized air. (a) The surface of the inflated PDMS balloon was imaged using 3D laser scanning microscopy, to measure the center height (*h*) of the PDMS balloon. (b) At air pressure (*P*) of 14 kPa, PDMS balloons of the same diameter (*D*) showed similar *h* on a single device, and *h* increased with *D*. Inset: PDMS balloon configuration. (c) Testing three devices showed similar *h* results (error bar: standard deviation of mean *h*), which supports the reproducibility of the fabrication method. Comparison between image-based measurement, finite element method (FEM) simulation,

and approximate analytical model (eqn (1)) shows good agreement between the measurement and simulation, and a possibility of using the model to predict PDMS balloon deformation. Red line: linear fitting line of image-based measurement.

Author Manuscript Author Manuscript Author Manuscript Author Manuscript

Author Manuscript Author Manuscript Author Manuscript Author Manuscript

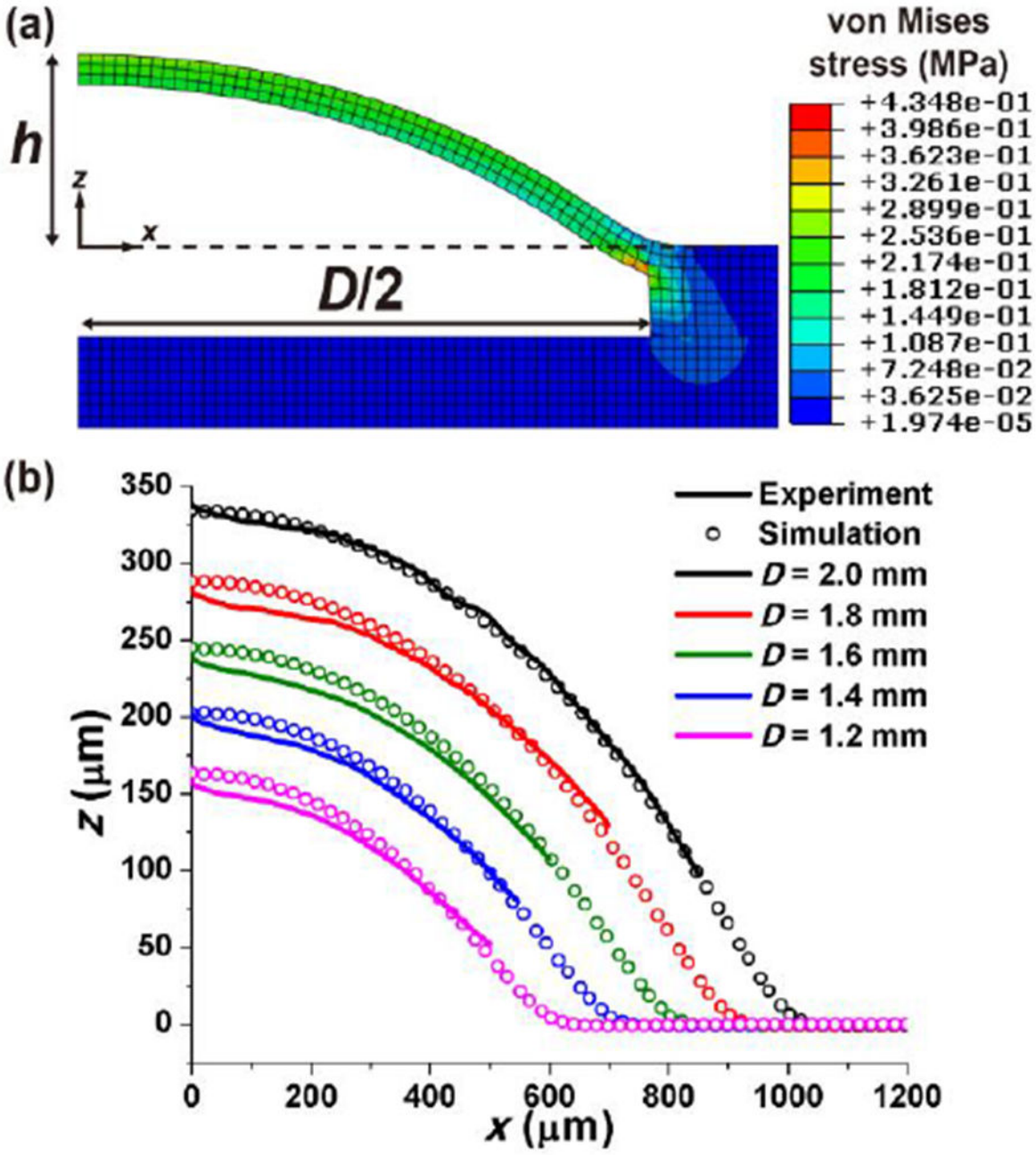


**Fig. 3.**

Finite element method (FEM)-based simulation of the expanded PDMS balloons at fixed air pressure of 14 kPa. (a) The simulation result of the 2.0 mm-diameter PDMS balloon provides detailed information on the deformation of the balloon such as stress concentration. *h* and *D* are the center height and diameter of the PDMS balloon, respectively. (b) Profiles of the expanded PDMS balloon measured by 3D laser scanning microscopy and FEM simulation show good agreement.

Author Manuscript Author Manuscript Author Manuscript Author Manuscript

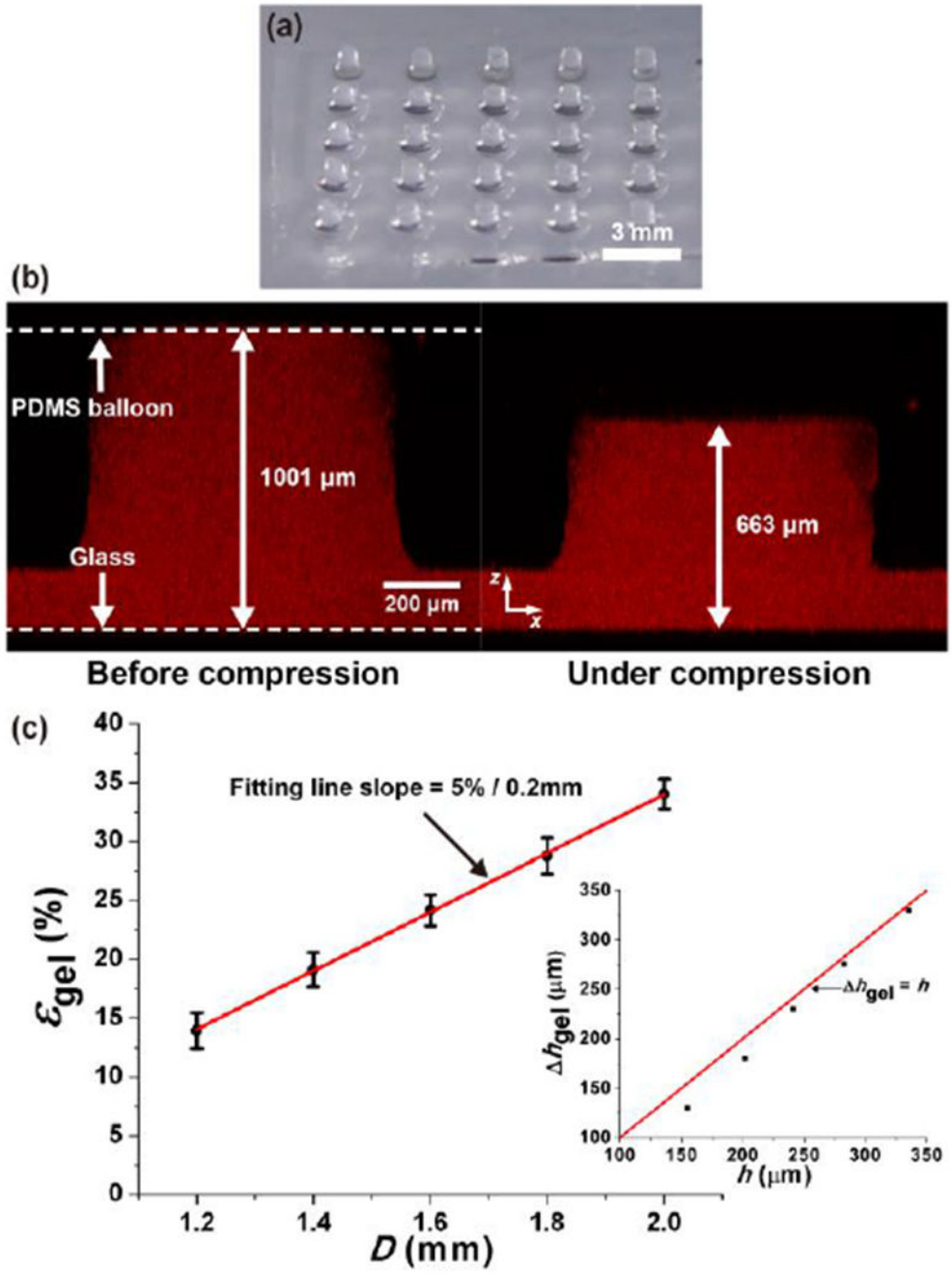


**Fig. 4.**

Alginate gel deformation under static compression. (a) Alginate gel constructs (diameter: ~800 μm, height: ~1 mm). (b) Alginate gel on the largest PDMS balloon ($D$ = 2.0 mm) before (left) and under (right) compression. Resultant strain is 33.8%. (c) Compressive strain of alginate gel ($\varepsilon_{gel}$) increased with the balloon diameter ($D$). Error bar: standard deviation. Red line: linear fitting line. The differences in $\varepsilon_{gel}$ are significant between all pairs ($p < 0.05$). Inset: Difference between the height change of the gel ($\Delta h_{gel}$) and the center height of the PDMS balloon ($h$) decreased with $D$ and approached $\Delta h_{gel} \approx h$ (shown as the red line).

Author Manuscript Author Manuscript Author Manuscript Author Manuscript

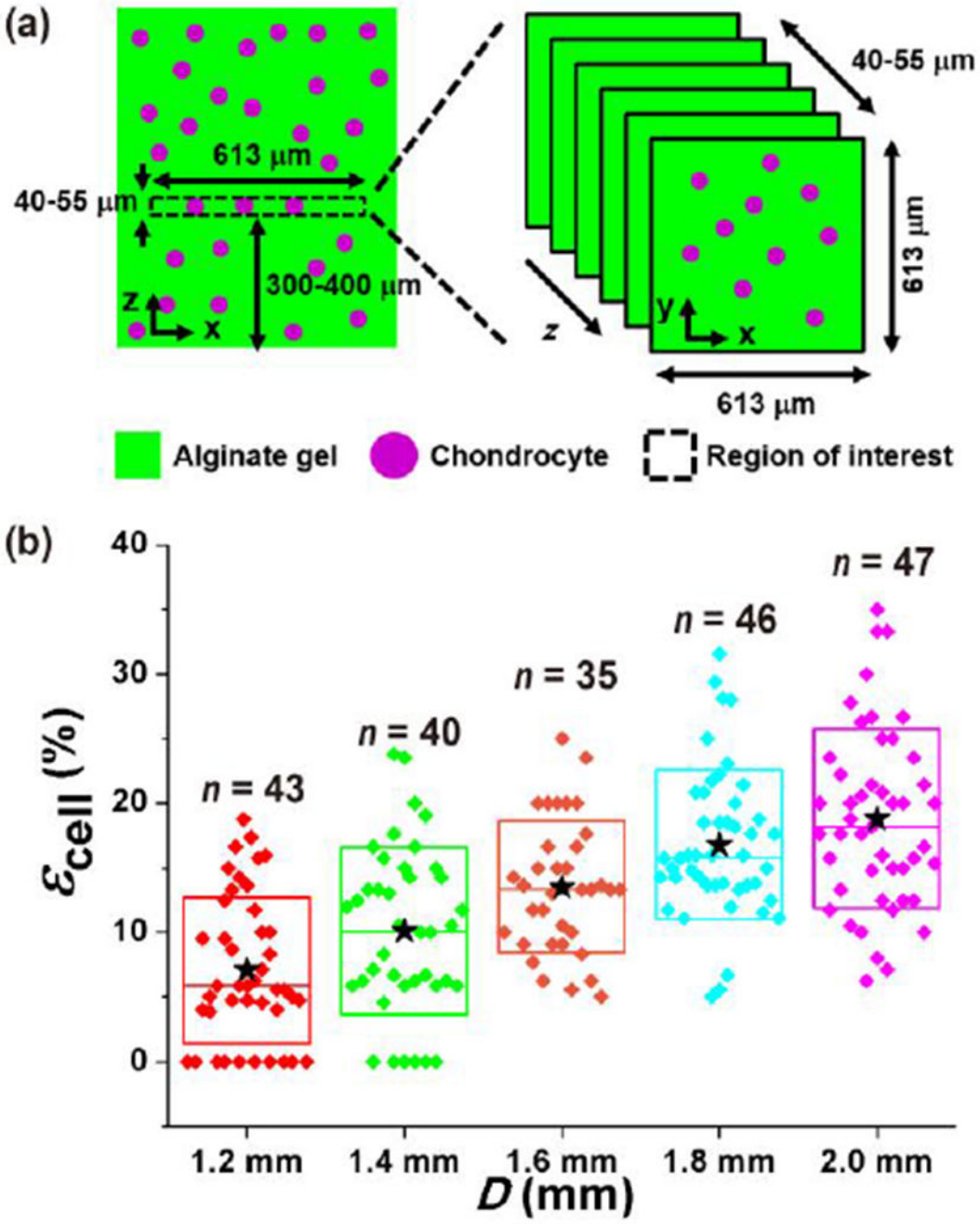


**Fig. 5.**

Chondrocyte deformation under static compression. (a) Imaged region in the alginate gel-chondrocytes construct was 613 μm × 613 μm × 40–55 μm ($x \times y \times z$) in size, and it was 300–400 μm from the gel base. (b) The compressive strain of chondrocyte ($\varepsilon_{cell}$) increased with the PDMS balloon diameter ($D$). The $\varepsilon_{cell}$ values of chondrocytes were significantly different in all pairs ($p < 0.05$) except adjacent pairs (not significant, $p > 0.05$). $n$: the number of chondrocytes. ★: mean values. ◆: each data points. Top and bottom lines of the box: standard deviation. Middle line of the box: median value.

Author Manuscript Author Manuscript Author Manuscript Author Manuscript

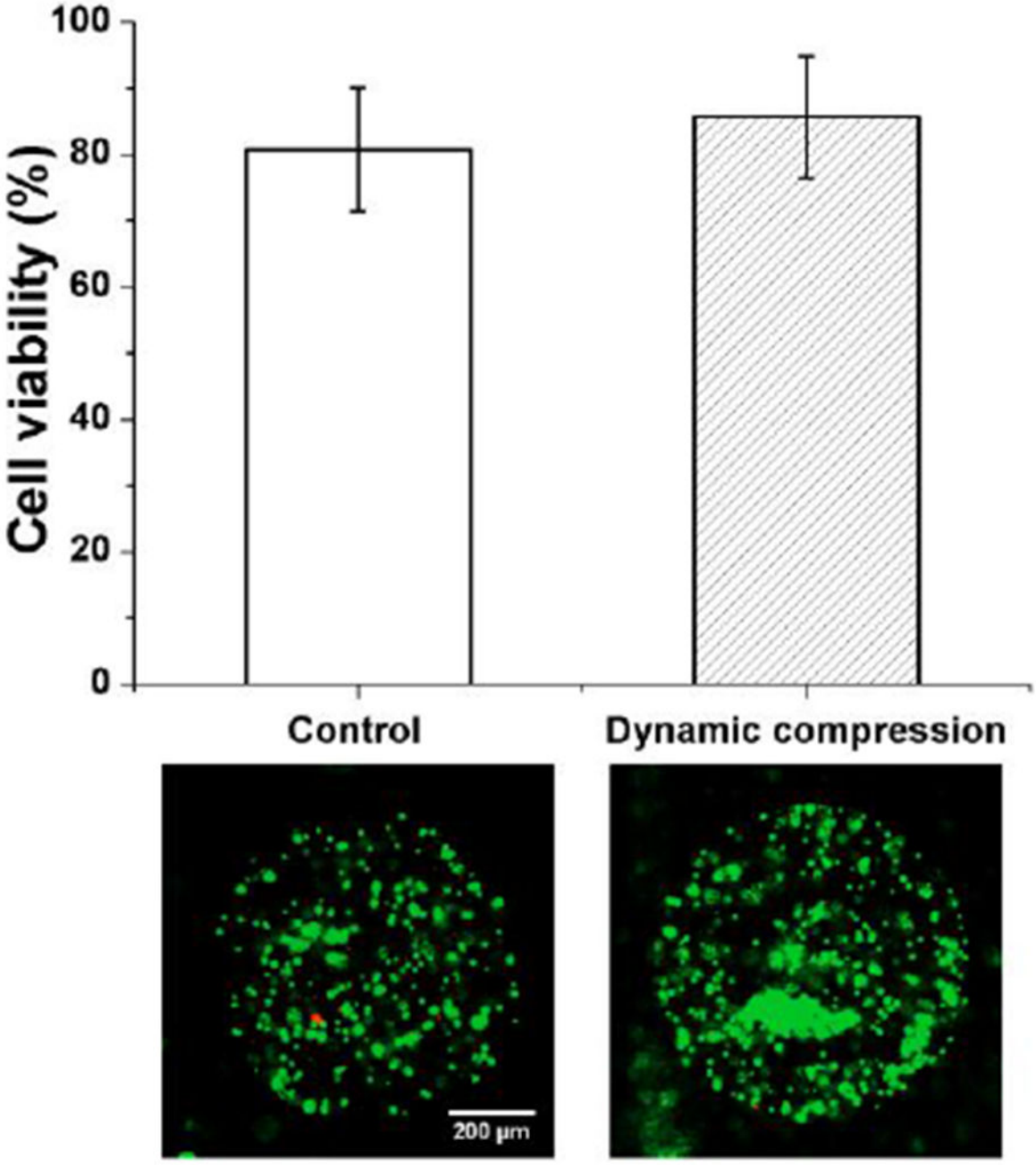


**Fig. 6.**

Chondrocyte viability without (control) and with 1 hour-long dynamic compression (1 Hz, 14 kPa air pressure, $n = 3$ devices). Error bar: standard deviation. Example images are shown below the plot. Green: live cells. Red: dead cells.

Author Manuscript

Author Manuscript

Author Manuscript

Author Manuscript

**Table 1.**

Summary of device performance.

| $D$ (mm) | PDMS balloon | Alginate gel | Chondrocyte |
|---|---|---|---|
| | $h$ (μm) | $e_{gel}$ (%) | $e_{cell}$ (%) |
| 1.2 | 155.2 ± 9.6 | 14.0 ± 1.5 | 7.1 ± 5.7 |
| 1.4 | 202.0 ± 11.5 | 19.1 ± 1.5 | 10.1 ± 6.5 |
| 1.6 | 241.3 ± 9.2 | 24.2 ± 1.3 | 13.5 ± 5.1 |
| 1.8 | 282.6 ± 8.2 | 28.8 ± 1.5 | 16.8 ± 5.8 |
| 2.0 | 335.4 ± 9.9 | 34.0 ± 1.3 | 18.8 ± 6.9 |

*D*: PDMS balloon diameter, *h*: PDMS balloon height, *e*: compressive strain